SPi	Journal Code				Article ID				Dispatch: 19.03.14	CE:
	E	S	P		3	5	6	3	No. of Pages: 13	ME:

EARTH SURFACE PROCESSES AND LANDFORMS
Earth Surf. Process. Landforms (2014)

Published online in Wiley Online Library
(wileyonlinelibrary.com) DOI: 10.1002/esp.3563

Bedload hysteresis in a glacier-fed mountain river

Luca Mao,[1]* Andrea Dell'Agnese,[2] Carolina Huincache,[1] Daniele Penna,[2,3] Michal Engel,[2,4] Georg Niedrist[4] and Francesco Comiti[2]

[1] Department of Ecosystems and Environment, Pontificia Universidad Católica de Chile, Santiago, Chile
[2] Faculty of Science and Technology, Free University of Bozen-Bolzano, Bolzano, Italy
[3] Department of Land, Environment, Agriculture and Forestry, University of Padova, Padova, Italy
[4] Institute for Alpine Environment, EURAC, Bozen-Bolzano, Italy

Received 4 March 2013; Revised 27 February 2014; Accepted 3 March 2014

*Correspondence to: Luca Mao, Department of Ecosystems and Environment, Pontificia Universidad Católica de Chile, Av. Vicuña Mackenna 4860, Macul, Casilla 306-22, Santiago, Chile. E-mail: lmao@uc.cl

ESPL
Earth Surface Processes and Landforms

ABSTRACT: Sediment transport during flood events often reveals hysteretic patterns because flow discharge can peak before (counterclockwise hysteresis) or after (clockwise hysteresis) the peak of bedload. Hysteresis in sediment transport has been used in the literature to infer the degree of sediment availability. Counterclockwise and clockwise hysteresis have been in fact interpreted as limited and unlimited sediment supply conditions, respectively. Hysteresis has been mainly explored for the case of suspended sediment transport, but it was rarely observed for bedload transport in mountain streams. This work focuses on the temporal variability in bedload transport in an alpine catchment (Saldur basin, 18.6 km^2, eastern Italian Alps) where bedload transport was monitored by means of an acoustic pipe sensor which detects the acoustic vibrations induced by particles hitting a 0.5m-long steel pipe. Runoff dynamics are dominated by snowmelt in late spring/early summer, mostly by glacier melt in late summer/early autumn, and by a combination of the snow and glacier melt in mid-summer. The results indicate that hysteretic patterns during daily discharge fluctuations are predominantly clockwise during the snowmelt period, likely due to the ready availability of unpacked sediments within the channel or through bank erosion in the lower part of the basin. On the contrary, counterclockwise hysteresis tend to be more frequent during late glacier melting period, possibly due to the time lag needed for sediment provided by the glacial and peri-glacial area to be transported to the monitoring section. However, intense rainfall events occurring during the glacier melt period generated predominantly clockwise hysteresis, thus indicating the activation of different sediment sources. These results indicate that runoff generation processes play a crucial role on sediment supply and temporal availability in mountain streams. Copyright © 2014 John Wiley & Sons, Ltd.

KEYWORDS: indirect bedload monitoring; bedload transport; sediment availability; mountain stream; snow and glacier melt

Introduction

Bedload transport is a key physical process determining fluvial geomorphology and morphodynamics, and its assessment is crucial for river management, stream ecology, and flood risk. However, a satisfactory bedload assessment in mountain stream is notoriously difficult to achieve. This is mainly due to the fact that mountain streams often feature stepped-like longitudinal profiles which produce tumbling flow conditions increasing energy dissipation (Comiti *et al.*, 2009) and the critical Shields stress needed to entrain sediments from the channel bed (Lenzi *et al.*, 2006). Also, mountain streams typically have high transport capacity/sediment supply ratios (Montgomery and Buffington, 1997) as they are characterized by a limited supply from sediment sources at the basin scale, and by a limited in-channel sediment storage, revealed by high armour ratios (Lenzi, 2001) and considerable degree of surface sediment organization (Zimmermann *et al.*, 2010). Because of these conditions, bedload formulas typically overestimate sediment transport by several orders of magnitude (Rickenmann, 2001; Rickenmann and Koschni, 2010). Prediction of bedload discharge becomes more accurate only at the highest water discharges, often associated with flood events under unlimited sediment supply due to disruption of step-pool sequences and activation of bank erosion and landslides (D'Agostino and Lenzi, 1999; Lenzi *et al.*, 2004; Rickenmann and Koschni, 2010).

Because bedload transport rates in mountain streams are closely related to the processes occurring at the channel and basin scales, which act at a range of temporal scales, continuous and long-term monitoring initiatives are needed to investigate bedload dynamics. However, direct measurements of bedload transport rates in mountain streams are difficult, expensive, and often dangerous to undertake (Gray *et al.*, 2010). To overcome these issues, surrogate methods, such as hydrophones, acoustic pipe sensors and geophones, are being increasingly used to measure bedload intensity and dynamics in mountain streams. In particular, geophones record the oscillation velocities produced by the impact of moving clasts colliding onto a metal plate (e.g. Vatne *et al.*, 2008; Turowski and Rickenmann, 2009; Rickenmann *et al.*, 2012), and acoustic pipe sensors record the acoustic signal generated by particles colliding on a air-filled metal pipe (Mizuyama *et al.*, 2003, 2010a, 2010b). To convert the signals recorded by these

instruments to actual bedload fluxes, direct bedload measurements are needed to obtain a calibration relationship (e.g. Rickenmann and McArdell, 2007; Mizuyama *et al.*, 2010a; Møen *et al.*, 2010).

Even if uncalibrated, indirect measurements can provide valuable insights into bedload fluctuations at small or long-term temporal scales (Turowski and Rickenmann, 2010). At the single flood scale, bedload rates have been found to exhibit hysteretic cycles with respect to water discharge due to a temporal lag between the two variables (Reid *et al.*, 1985; Rickenmann, 1994; Rickenmann *et al.*, 1998; Turowski *et al.*, 2009). Hysteresis is clockwise if the peak of bedload transport occurs before the peak of water discharge, whereas the opposite (i.e. bedload peaking after water discharge) depicts a counterclockwise hysteretic loop. Clockwise hysteresis at the single event scale can be the result of a breakage of an armour layer (Kuhnle, 1992), of the early activation of sediment sources (Habersack *et al.*, 2001), or due to the fact that sediments in the channel bed are still unorganized due to the occurrence of previous high-magnitude flood events (Reid *et al.*, 1985). On the contrary, counterclockwise hysteresis can result from an armour or bedforms breakage after the peak of water discharge (Kuhnle, 1992; Lee *et al.*, 2004), or from the consolidation of surface sediments in the channel due to the occurrence of previous low-magnitude flood events (Reid *et al.*, 1985). A number of laboratory experiments have demonstrated that clockwise hysteresis of bedload transport is a result of a lack of sediment supply (Hassan *et al.*, 2006), and of dynamics of pool scour and fill (Humphries *et al.*, 2012), and bed restructuring (lower vertical roughness, clasts rearrangement), which causes lower sediment mobility and sediment transport rate during the falling limb of hydrographs (Mao, 2012).

Bedload hysteresis at temporal scales larger than single flood events has been hardly explored in the literature. More evidence is available for suspended sediment transport, and different suspended sediment transport rate–water discharge relationships have been developed depending on seasonal period or hydrological patterns (e.g. Horowitz, 2003). Recently, Araujo *et al.* (2012), recognizing significant differences in suspended sediment transport due to seasonality, developed a mixed-effects model to predict suspended sediment concentration that proved to perform better than simple rating curves. Seasonality in suspended sediment transport can reveal important dynamics of sediment sources at the basin scale, allowing to distinguish periods characterized by transport-limited and supply-limited conditions (Fuller *et al.*, 2003). Seasonality in suspended sediment transport has been related to rainfall intensity (Kwaad, 1991), type of storms (Alexandrov *et al.*, 2007), soil moisture (Giménez *et al.*, 2012) and vegetation cover dynamics (Steegen *et al.*, 2000). Wulf *et al.* (2012) found dominance of counterclockwise hysteresis of suspended sediment transport in the Sutlej River (western Himalaya), and related this to higher glacial sediment evacuation during late summer, stressing the importance of ready-available sediments in the upper portion of the basin that can be transported downstream by glacier melting and rainfall events. Similarly, Tananaev (2012) depicted the role of permafrost conditions in determining hysteretic effects between suspended sediment concentration and water discharge. Analysing the effects of snowmelt on suspended sediment transport in a Japanese headwater basin, Iida *et al.* (2012) demonstrated that more than half of the annual suspended sediment load occurred during snowmelt. Also, clockwise hysteresis dominated in the early snowmelt period as a result of readily available sediments within the channel network, whereas counterclockwise hysteresis was observed only in the late stage of the snowmelt period. Focusing on bedload dynamics and morphological changes in a pro-glacial river, Lane *et al.* (1996) reported the dominance of scour on the rising limb of the hydrograph and deposition on the falling limb, highlighting the effects of glacier-derived sediment supply and channel adjustments on bedload response to single daily discharge cycles.

The present paper reports on the temporal dynamics of bedload transport at the seasonal scale in a glacierized mountain basin where bedload transport is monitored by an acoustic pipe sensor. The main aim is to characterize the dynamics of sediment transport during snowmelt and glacier melt periods, and to assess the relevance of rainfall events in determining the activation of sediment sources at the basin scale. This paper highlights the great value of continuous measurements of bedload transport provided by surrogate devices – even when not calibrated – in order to explore the degree and temporality of bedload fluctuations.

Materials and Methods

The study area is the upper Saldur basin (18.6 km^2, eastern Italian Alps), whose elevations range from 2150 m above sea level (a.s.l.) (location of the monitoring site) and 3738 m a.s.l. (Figure 1). The main glacier hosted in the basin lies between approximately 2700 and 3700 m a.s.l., with a current extent of 2.8 km^2 (it was 4.9 km^2 in the 1800s at the peak of the Little Ice Age). Presently, 15% of the basin area is glacierized. Due to its inner-alpine position, the mean annual precipitation in the lower valley is lower than 530 mm at 1600 m a.s.l. However, a strong lapse rate leads to 700-1000mm at the higher altitudes of the basin. In the study area, precipitation typically occurs as snowfall from November to late April, but snow storms can occur also during the summer at the higher elevations. Typically, snow cover is almost complete over the entire study basin until late April–early May, when the melting season begins. At the beginning of July snow cover in recent years ranges between 10% and 25%, whereas at the end of the summer only a few patches of snow are present at the higher elevations, on the glacier surface or in sheltered couloirs.

The entire Saldur basin belongs to the Ötztal-Stubai complex and consists mainly of orthogneiss (Habler *et al.*, 2009). During the Pleistocene it was entirely glaciated and glacial erosion has imparted the typical U-shaped form of the upper basin (Figure 2). Several rock-glaciers and large moraines are found in the basin, but their connectivity to the main channel appears to be rather limited. Other sediment sources are represented by talus slopes (mostly located at the higher elevations), shallow landslides (of limited extent) and large alluvial fans reaching the valley bottom from the steep tributaries. Permafrost is most probably present at elevations higher than 2600–2800 m a.s.l., depending on local conditions (Boeckli *et al.*, 2011). Shrubs and alpine grass essentially represent the only vegetation cover up to 2700 and 2400 m a.s.l. on south and north faced slopes, respectively.

The longitudinal profile of the river (from the glacier snout at 2730 m a.s.l. to the monitoring section, for a length of 4.58 km, see Figure 3) displays a series of valley steps, the largest and steepest of which are in bedrock, the others due to the alluvial fans built by the tributaries. The average channel slope is 12.6%, but this varies from about 30% of bedrock reaches to about 5% along the reaches immediately upstream of the valley steps, where the Saldur River widens and attains a wide (30–50m) braided pattern. However, single-thread reaches are overall dominant, with slopes about 6%, channel width of about 4–6 m, featuring step-pool and cascade characteristics but with occasional glide-run units and lateral bars. The reach

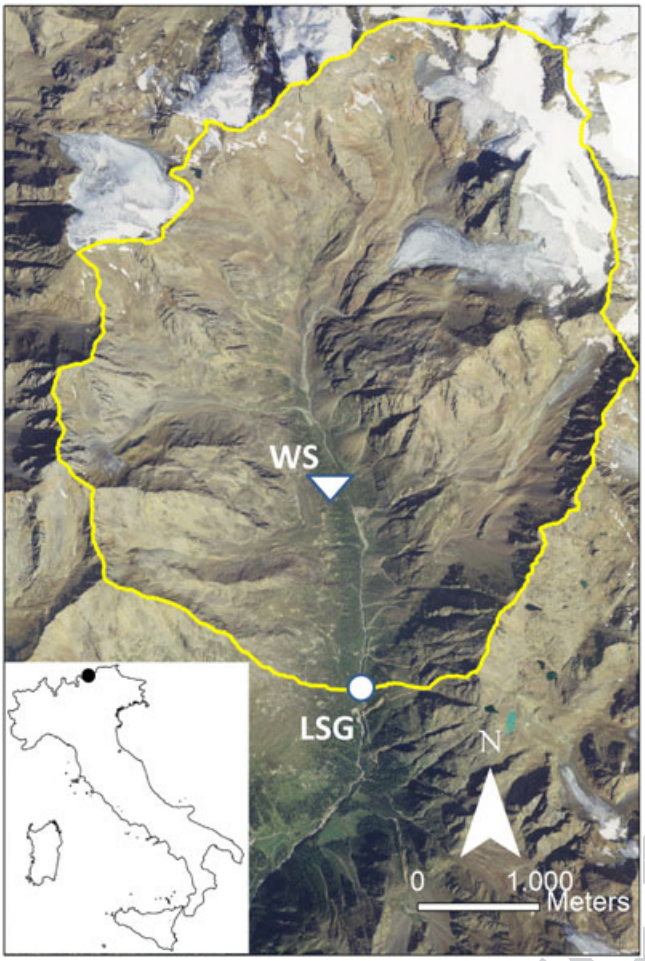

Figure 1. Location and map of the Saldur River basin closed at the section LSG (lower stream gauge), where water and bedload monitoring discussed in this paper was carried out. The location of the weather station (WS) is also shown.

Figure 2. Downstream view of the U-shaped Saldur glacier valley.

just upstream of the monitoring station is confined by the adjacent hillslopes and features a 6% slope, 5–6 m width, and a bed morphology transitional from plane-bed to step-pool. Surface grain size distribution is characterized by the following percentiles (in millimetres): D_{16} = 43, D_{50} =108, D_{84} = 304, and D_{90} = 417. The bed appears rather armoured, as subsurface D_{50} and D_{84} measured after removing the first layer of sediments (approximately 150 cm thickness) are 15 and 46 mm, respectively.

The monitoring station was installed at 2150 m a.s.l. (lower stream gauge, LSG, in Figure 1) at the narrowest section (3 m)

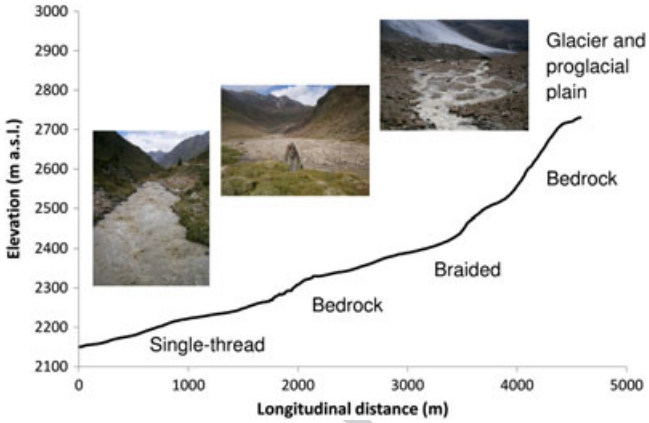

Figure 3. Longitudinal profile of the Saldur River from the monitoring site to the glacier, depicting relevant changes in slope and associated morphological pattern of the main channel.

along the upper Saldur River, where accessibility through an unpaved road is available for 4WD vehicles, and channel banks are stabilized by very large boulders. In late May 2011, the department of Hydraulic Engineering of the Autonomous Province of Bozen-Bolzano placed a wooden log transversally in the channel bed, anchored against the boulders of the banks and stabilized by a sort of boulder ramp (Figure 4). A slot was previously carved into the log to host half the diameter (5 cm) of a 0.5 m long acoustic pipe sensor, manufactured by Hydrotech Company (Japan), the same measuring instrument deployed in several Japanese streams since the 1990s (Mizuyama *et al.*, 2003, 2010a). Even if the instrumented cross-section is 3 m wide and the pipe 0.5 m long, the horizontal wooden log on the bottom provides a regular shape to the cross-section, likely making the impulses registered by the pipe representative of the whole section.

The Japanese acoustic pipe sensors is a steel, air-filled pipe with a microphone inside which detects the acoustic vibrations induced by hitting particles. Vibrations are amplified by a pre-amplifier inside the pipe and then transmitted to a converter, which generates a voltage processed through a six-channel band-path filter. The impulses generated by particle collisions are recorded in the datalogger when the output from a channel exceeds a given threshold (Mizuyama *et al.*, 2010a). The datalogger and converter were installed in a case on the river bank, where a solar panel and a battery supplied the required power to the system. The number of impulses for each channel is recorded at one minute intervals in the datalogger. However, in order to interpret bedload dynamics at intermediate timescales and to match the resolution of flow stage records, for the analysis presented here impulses were analysed after averaging the signals over 10 minute intervals. The voltage thresholds for registering collisions at the different channels are the same used by Mizuyama *et al.* (2010a, 2010b). The pipe sensor functioned without major interruptions from July to September 2011. The calibration of the pipe sensor data through bedload samples collected using a portable bedload trap (Bunte *et al.*, 2004) is in progress, and hysteresis cycles will be analysed in this paper based solely on the number of impulses per unit of time. At the same cross-section, water stage is measured every 10 minutes by a pressure transducer, and a stage–water discharge relationship was derived based on 82 discharge measurements carried out in the period 2011–2013 using the salt dilution method (slug injections), from low (0.6 $m^3\ s^{-1}$) up to near-bankfull flows (4.5 $m^3\ s^{-1}$). Meteorological data (temperature and precipitation) are acquired by a weather station at 2330 m a.s.l. run by the EURAC research centre.

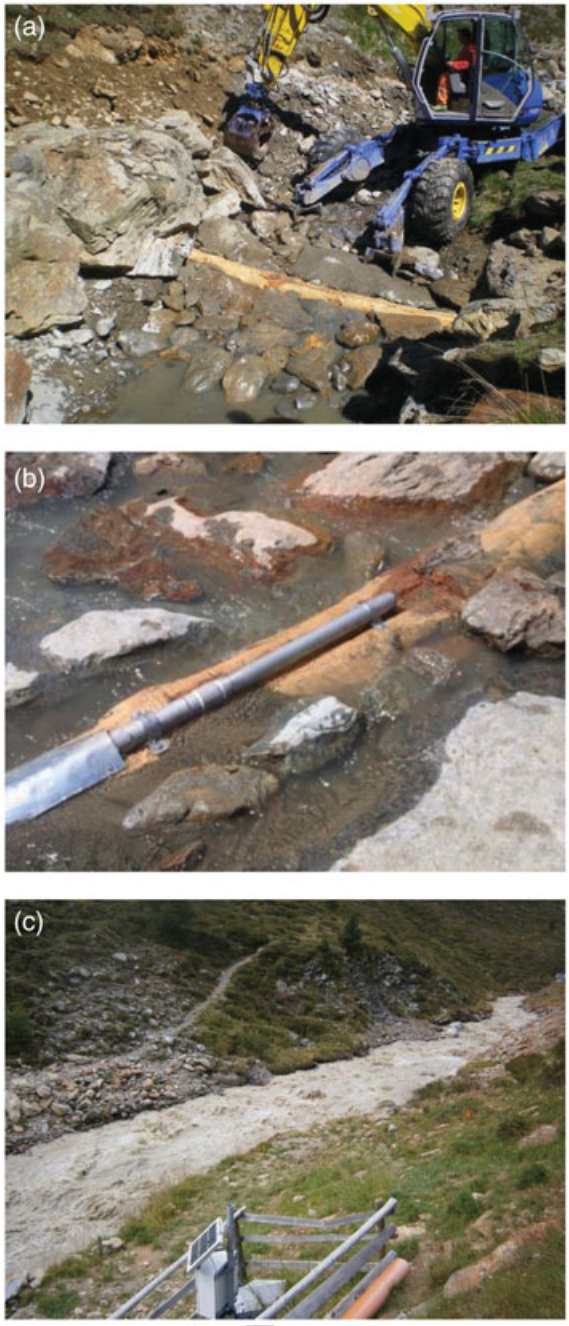

Figure 4. Installation of the acoustic pipe sensor in the monitoring site (a). The geophone was fixed in a slot carved in a transversal log, which leave approximately half of the 0.5 m-long pipe protruding into the flow (b). A view of the Saldur River at a near bankfull flow (4 m^3 s^{-1}) (c).

In addition, in order to investigate the seasonal variation of water sources to runoff in the Saldur basin, a tracer experiment based on water stable isotopes (^2H and ^{18}O) and electrical conductivity data was carried out between April and October in 2011 and 2012. Bulk precipitation was collected at three locations in the catchment, at 1826, 2154 and 2336 m a.s.l. Also, grab water samples were collected on a monthly basis from four springs, four tributaries and at seven sections along the stream (including the monitoring section). Snow and snowmelt (from dripping snow patches) was sampled occasionally in 2011 and 2012, and glacier meltwater samples were collected on three occasions in the summer of 2012 from rivulets in the lower portion of the main glacier tongue. Isotope analysis was performed at the Isotope Hydrology Laboratory at the University of Padova by means of laser absorption spectroscopy (Penna *et al.*, 2010, 2012), and by means of mass spectrometry at the Free University of Bozen-Bolzano. A detailed description of the experimental design as well as preliminary results of the isotopic investigation in the Saldur basin can be found in Penna *et al.* (2013). For the purpose of this paper only the temporal distinction between snow and glacier melt flow in the main channel derived by the tracer-based analysis is relevant to discuss the occurrence of different hysteresis cycles.

Results

Hydrological characteristics of the study period

During the period when the acoustic pipe sensor was operational (1 July–25 September 2011, Figure 5), mean daily temperature (measured at 2330 m a.s.l.) was 8.6 °C, which means a 0 °C level at 3600 m a.s.l. (assuming a standard lapse rate of 6.5 °C/1000 m) with practically all the catchment in melting conditions. However, a significant variability was observed within this period. In fact, daily average temperatures ranged from −2.1 to 15.3 °C, with instantaneous extremes reaching −4.3 and 21.7 °C on 19 September and 22 August, respectively. Nine relevant rainfall events (defined here as having a daily cumulated value > 10 mm) occurred during the study period, the largest of which (35 mm) took place on 4–5 September. On 18 September, a precipitation of nearly 60 mm occurred mostly as snowfall (see the temperature drop in Figure 5), with a negligible discharge peak and the snow cover in the basin melting within 3–4 days. Overall, the total depth of precipitation in the study period was 270 mm. **F5**

Water discharge ranged from 0.9 to approximately 10 m^3 s^{-1} during the 3–4 September flood, with significant daily fluctuations due to snow and glacier melt (Figure 5). However, some uncertainty (probably ±20%) does exist for the highest value, as the flow rating curve was built with discharge measurements only up to about 4 m^3 s^{-1}. Indeed, the 3–4 September flood is likely a non-ordinary event (i.e. more than 2–3 years of recurrence interval) based on information provided by the Hydrographic Office of the Autonomous Province of Bozen-Bolzano. No other relevant rainfall-induced events occurred in the study period.

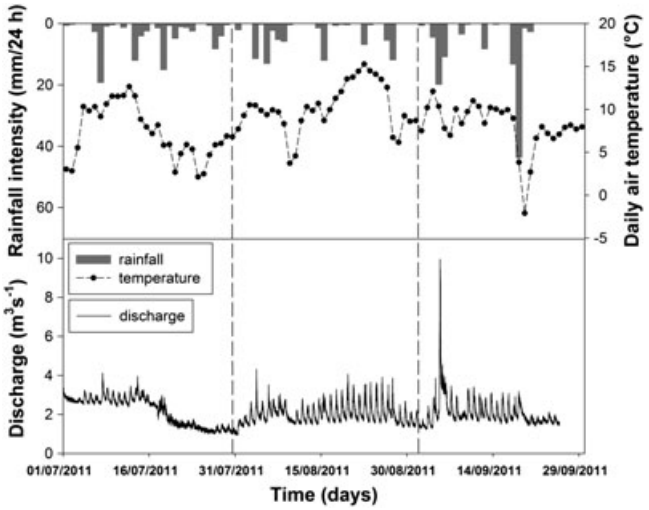

Figure 5. Daily mean air temperature and rainfall as measured by the weather station located at 2300 m a.s.l (WS in Figure 1), and discharge measured at the monitoring site in LSG. Three periods characterized by different runoff-generation processes are defined as snowmelt (a), glacier melt (b), and late glacier melt (c).

Melting flows reached up to approximately 4 $m^3 s^{-1}$, both in July and August, which appear to correspond to a stage slightly lower than bankfull conditions, based on visual assessment in the river reaches featuring floodplain pockets (Figure 4c).

The temporal dynamics of discharge, air temperature, precipitation and water isotopic characteristics led to the identification of four different phases within the study period, each associated with different main contributors to runoff. The first period (1–16 July) was characterized by relatively high air temperatures (> 10 °C) and moderate daily discharge fluctuations (< 0.6 $m^3 s^{-1}$), as low flows were always higher than 2–2.5 $m^3 s^{-1}$. Field observations support the evidence that snowmelt contribution to this period was dominant as the glacier was still significantly covered by snow. Remote sensing data used in Engel *et al.* (2013) reveal a snow cover of around 8–10 km^2 for the study area. From 18–31 July, the temperature decreased substantially, causing a sharp reduction in the average runoff with very little daily fluctuations as snowmelt was probably limited to short times during the warmest hours of the day. Overall, even if characterized by two phases, from 1 to 30 July the dominant process of runoff generation was snowmelt but with some contribution from the glacier, most likely from its lowest snow-free part. From 30 July, a sudden increase in the air temperature to values similar to the first half of July produced a marked rise in discharge. Only after mid-August – when air temperatures remained very high for a prolonged period – daily maxima in water discharge attained and exceeded early July values. Daily fluctuations in late August were the largest of the entire study period, as flow rose from 1.5 $m^3 s^{-1}$ in the early mornings to 4 $m^3 s^{-1}$ in the evenings. The runoff regime for the entire period from 1 August to 2 September can be ascribed to intense glacier melting, with some contribution from snowmelt especially in early August. After the 3–4 September flood event, lower air temperatures decreased daily fluctuations as daily maxima reached about 3 $m^3 s^{-1}$ whereas minima were similar to August. The runoff regime in the period 2–25 September (excluding the few days when temperature dropped below zero, Figure 5) can be described almost entirely to late glacier melt.

The identification of three main periods (i.e. roughly corresponding to July, August and September) featuring different runoff sources is also supported by isotopic data. During fall and winter the background $\delta^{18}O$ value of the stream at the monitoring section ranged between −13.9 ‰ and −14.3 ‰. However, from late spring until mid-July 2011, $\delta^{18}O$ values were on average relatively depleted (−15.0 ‰, $n = 10$), likely skewed towards the snowmelt signal (average of −15.5 ‰, $n = 26$). Conversely, during late summer, stream values were on average relatively more enriched (−14.4 ‰, $n = 7$) likely reflecting the input derived by glacier melt water (average −14.4 ‰, $n = 16$). Although less clearly, the seasonal variability of electrical conductivity confirmed this distinction. Water samples until mid-July had an average value of 177 μS cm^{-1} ($n = 10$) whereas in late August values were on average lower (152 μS cm^{-1}, $n = 7$). Although other water sources could have masked such a difference (e.g. local groundwater seepage or contribution by tributaries) this likely reflects the difference in average electrical conductivity between snowmelt (13.3 S cm^{-1}, $n = 19$) and glacier melt water (2.1 μS cm^{-1}, $n = 14$).

Bedload–water discharge relationships

Overall, 84 complete fluctuations of water discharge can be identified from 1 July to 25 September. Most of them occurred at a daily scale (24 hours approximately) and are clearly due to snow or glacier melting, since no precipitation occurred. However, seven of these fluctuations exceeded 41 hours and are related to significant rainfall events or minor rainfall during glacier melt events.

Variations in bedload impulses recorded by the pipe sensor were associated with each fluctuation of water discharge. Because the signal from the channels of the most sensitive pipe sensors (channels 1 and 2) become dampened at relatively low discharges, and less sensitive channels (channels 5 and 6) do not register impulses at lower discharges due to the relatively small clast size transported by these flows (Mizuyama *et al.* 2010a, 2010b), channel 4 was used in order to characterize the temporal fluctuations of bedload transport. Other channels were used to better interpret hysteretic patterns for particularly low magnitude events (channel 3) or for the higher discharges (channel 5) during the 4–5 September flood event.

Water discharge and impulses collected by the pipe sensor were used to identify the hysteretic cycle of each 'event' (i.e. daily fluctuation). Figures 6a and b shows an example of counterclockwise hysteresis on the 23 August, when most of the bedload transport appears to occur during the falling limb of the daily hydrograph generated by intense glacier melt. Interestingly, a similar discharge fluctuation peaking at 4 $m^3 s^{-1}$ and occurring the day after resulted in a bedload peak occurring during the rising limb of the hydrograph, thus exhibiting a clockwise loop (Figures 6c and d).

Overall, 43 events exhibit a clockwise and 36 a counterclockwise pattern (Figure 7). No obvious hysteresis cycle could be identified for five events either for gaps in the acoustic pipe data (due to sedimentation problems) or because evidence of hysteresis was absent (i.e. similar relationship in discharge versus bedload during both rising and falling limbs). Figure 7 summarizes the hysteretic pattern of each daily event. It appears that clockwise events are concentrated in the early portion of the study period, whereas counterclockwise events are more common later, during the glacier melt period. When the three main periods characterized by different processes dominating the generation of runoff are considered, 86% of the events are clockwise during the snowmelt-dominated period of July. In contrast, < 50% of events are clockwise in August when glacier melt had most likely become predominant, and finally during the late glacier melting period in September this percentage reduces to 14% (Figure 8).

Five rainfall events occurred during the glacier melt period (i.e. August), and it is worth observing the different bedload hysteretic pattern of these events, which involve runoff generation at the basin scale. In fact, hysteresis was clockwise in 61% of the events occurring in August during a day with rainfalls, and in 83% of the events if rainfall occurred the same day or the day before, indicating the influence of rainfall-generated events on bedload hysteretic pattern.

Hysteretic patterns of single events thus seem to reveal differences in the temporal dynamics of bedload. Besides, even if uncalibrated against direct bedload measurements, absolute values of impulses registered by the acoustic pipe can provide information on the magnitude of bedload transport rate. Figure 9 shows bedload pulses as registered by channel 4 in the three periods analysed earlier. Despite the likely dampening of the acoustic signal at channel 4 during the highest flows during the 3–4 September flood, it appears that bedload transport rate became higher proceeding from July to September, i.e. moving from a snowmelt to glacier melt dominated periods. Such a strong seasonal difference in bedload transport rates is confirmed by direct measurements carried out in the Saldur River in the period 2011–2013 (Comiti *et al.*, 2013).

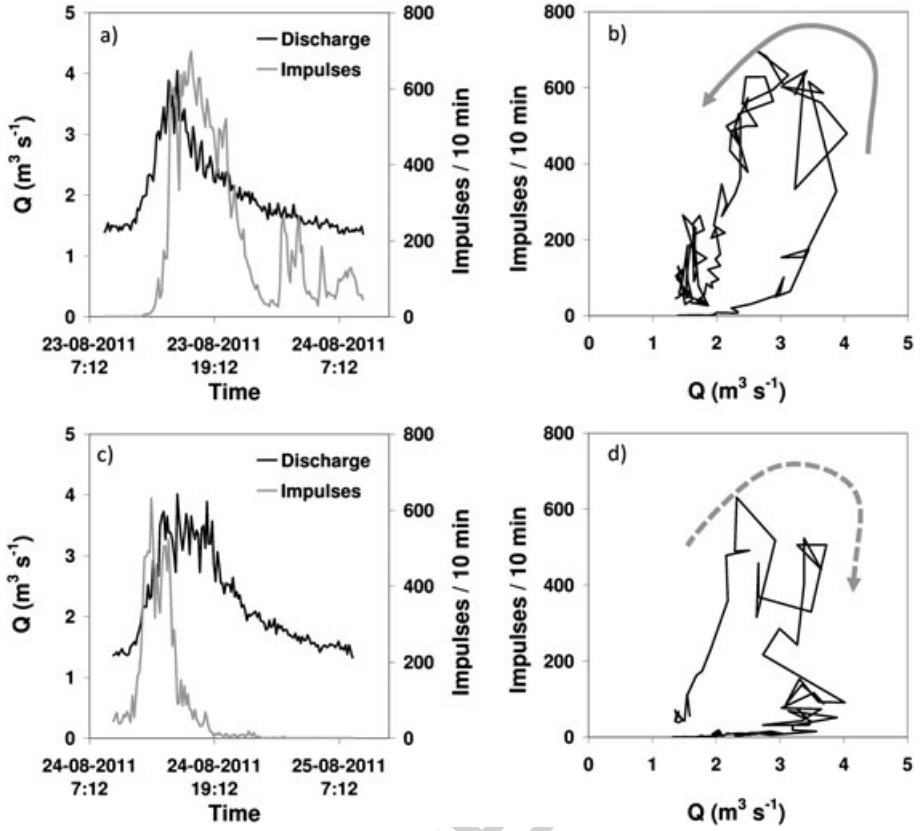

Figure 6. Water discharge and bedload impulses measured by the geophone's channel 4 registered on 23 August 2011 (a) and 24 August 2011 (c). On the former day the bedload peak occurred after the water discharge peak, creating a counterclockwise hysteresis (b), whereas on the latter the peak of bedload occurred before the discharge peak producing a clockwise hysteresis (d).

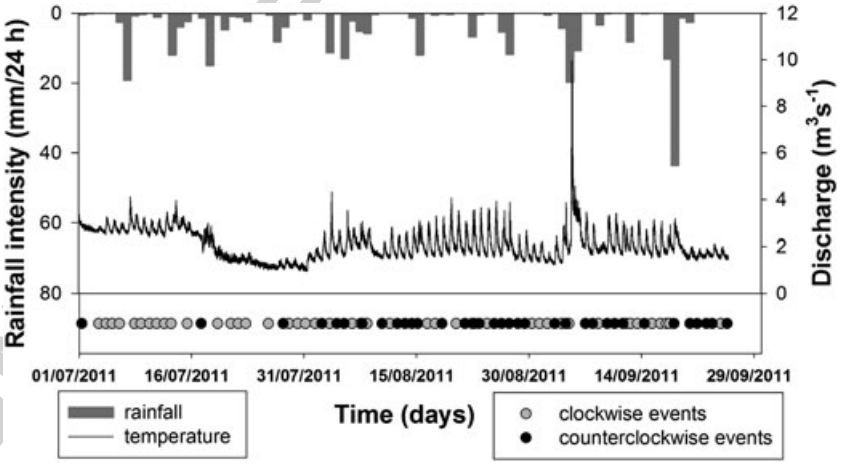

Figure 7. Clockwise and counterclockwise bedload events over the study period.

Discussion

Bedload dynamics during snowmelt

Bedload impulses on the acoustic pipe sensor installed in the Saldur River revealed how complex are the temporal dynamics of coarse sediment transport associated with melting (from snow and glacier) flow events. Overall, during the snowmelt-dominated period (i.e. approximately corresponding to June and July in the Saldur River, Penna *et al.*, 2013) the clockwise hysteretic pattern dominates, i.e. bedload transport peaks before water discharge. Very little evidence of bedload hysteresis during snowmelt periods is available in the literature. For example, Vatne *et al.* (2008) observed clockwise hysteresis of bedload transport measured using impact sensors during diurnal discharge fluctuations of spring floods (due to snowmelt) in central Norway. Clockwise hysteresis in bedload transport during snowmelt floods was also reported by McNamara and Borden (2004), who installed motion-sensing radio transmitters in single coarse grains, observing that tagged particles are more likely to move on the rising than on falling hydrograph limbs. Also, the clockwise pattern is in agreement with observations of suspended sediment transport in small mountain basins. For instance, Lana-Renault *et al.* (2011) found clockwise daily suspended sediment concentration-discharge loops during the snowmelt period in a high-elevation basin of

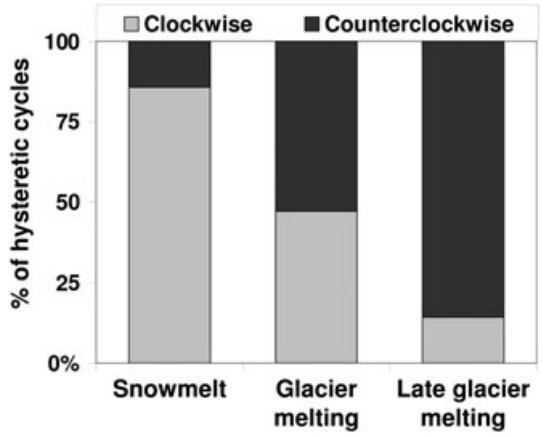

Figure 8. Proportion of clockwise and counterclockwise events during the snow melting (1–30 July), glacier melting (31 July–1 September), and late glacier melting (1–25 September) time spans.

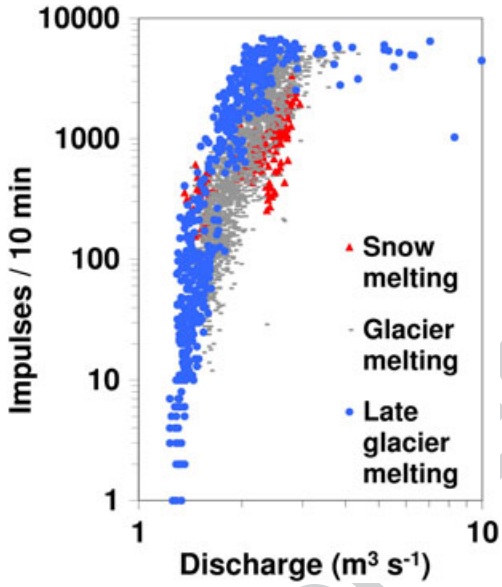

Figure 9. Bedload impulses as registered by channel 4, showing different relationships between bedload transport and water discharge for the three periods featuring different runoff sources.

the central Pyrenees. Similarly, Iida *et al.* (2012) found strong clockwise hysteresis for suspended sediment transport in the early stage of the snowmelt period in the coastal region of the Honshu Island, and they related it to the high availability of fine sediments in the channel bed. As shown by Priesnitz and Schunke (2002) and Forbes and Lamoureux (2005), during the snowmelt season the water temperature increases to a range that allowed thermal erosion of the bed and banks, thus increasing sediment availability for transport. Further studies relate clockwise hysteresis with ready availability of sediment sources within or close to the channel (Klein, 1984; Hudson, 2003; McDonald and Lamoureux, 2009).

However, the interpretation of why bedload clockwise loops dominate during snowmelt in the Saldur River is not straightforward, as it could be due to a combination of different processes, namely the ready supply of sediment from sources close to the monitoring station, and the fact that particles in the channel bed are ready movable in early summer. Indeed, during June–July (not only in 2011 but also in 2012 and 2013) relevant bank erosions of floodplain pockets – covered by grass vegetation – were noted in the single-thread reach upstream of the station during the rising limb of diurnal discharge fluctuations. Most likely, banks there become destabilized by spring freeze–thaw cycles, snowpack sliding, and by saturated conditions following snowmelt. The upper channel reaches featured more stable banks for a combination of prolonged snow cover and reduced unit stream power, as the channel there is wider. The presence of clockwise loops for many diurnal cycles in July may be linked to the capacity of the river to evacuate the sediment eroded from the banks out of the study basin within a few hours. This likely happens because the location of sediment sources is close to the station and thus sediment-water kinematic time lag is not relevant. This interpretation would seem compatible with evidence provided by the earlier mentioned works on suspended sediment transport hysteretic cycles during snowmelt.

In addition, clockwise loops during the snowmelt-dominated period could also be attributed to processes occurring at the grain-scale, i.e. loose grain packing and poor grain sheltering due to unstructured bed surface (Reid *et al.*, 1985). In the Saldur River, glacier-derived sediments are probably left poorly structured in the bed at the end of the melt period, and freeze–thaw processes on exposed surface sediments during late autumn–early winter could contribute to de-structuring even further of surface clusters and grain imbrication. In the measuring section, the channel bed is unlikely to freeze completely during winter (developing the so-called bedfast ice as it is known in the un-floating ice stabilizing sediment bed in arctic environments), which would have led to counterclockwise hysteresis of bedload transport (Priesnitz and Schunke, 2002; Best *et al.*, 2005). Instead, early snowmelt discharges provide the bed with fine sediments (Lana-Renault *et al.*, 2011; Iida *et al.*, 2012), which in a gravel bed surface could make sediments relatively more mobile (Wilcock *et al.*, 2001). Indeed, visual inspections of the channel bed in early spring (before snowmelt started) show abundant sand over a loose gravel framework (Figure 10a), supporting the hypothesis that dominant clockwise hysteresis in the snowmelt period is partly due to unpacked surface sediments close to the monitoring station.

Bedload dynamics during glacier melting

In August 2011, when glacier melt most likely became the predominant source of runoff in the Saldur River but snowmelt was still relevant (Penna *et al.*, 2013), water-bedload impulses relationships do not show any clear dominance of clockwise versus counterclockwise patterns (Figure 8). Interestingly, when intense rainfall events occurred during this period, these led to predominantly clockwise loops within one or two days after rainfall. This pattern might indicate a sudden connection – not present during melt flows – with active sediment sources at the basin scale, which most probably come from relatively low elevation tributaries (where precipitation was in the form of rainfall and not snowfall) featuring steep, easily erodible slopes and entering the main channel close to the LSG station (Figure 10b).

During the late glacier melting in September, a predominance of counterclockwise loops – punctuated by clockwise cycles – is observed, possibly suggesting that a marked change in the location of sediment supply takes place after the snowmelt is almost complete also at the higher elevations and on the glacier (Table I). In particular, the peri-glacial area at 2700–2900 m a.s.l. (Figure 3), where the Saldur River features a braided pattern on loose and relatively fine moraine material – replenished by frequent inputs during warm late summer days from adjacent rock-glaciers and dead ice masses – is most likely a relevant source of sediment during this period based

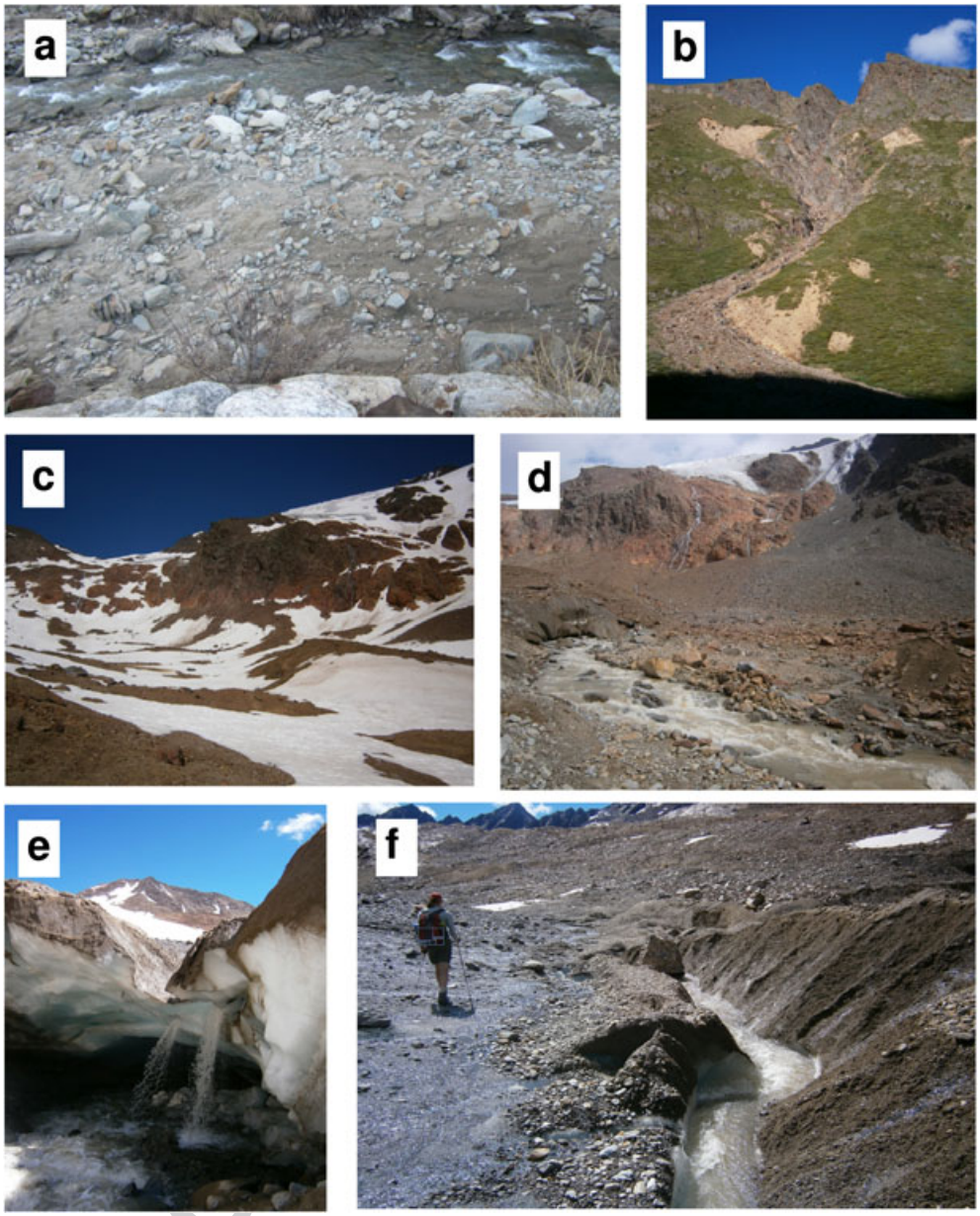

Colour online, B&W in print

Figure 10. Images from the Saldur River basin: (a) loose gravel sediments and sand patches observed in early spring before snowmelt starts; (b) one of steep tributaries likely to deliver sediments into the Saldur River just upstream of LSG during intense rainfall events; (c) and (d) views of the peri-glacial area at about 2800 m a.s.l. in mid July and late August, respectively; (e) a large tunnel within the tongue of the glacier, with the a branch of the Saldur River running through it, in August; (f) a supra-glacial channel flow beside the current lateral moraine in August., observed to carry abundant coarse sediments.

Table I. Runoff generation processes and bedload transport characteristics in the different seasons in the Saldur River

Season	Main runoff source	Sediment transport capacity	Prevalent sediment supply sources	Relative bedload transport	Dominant water–bedload relationship
Winter/ early spring	Groundwater	No competent flows	In-channel	No bedload	
Late spring/ early summer	Snowmelt	Limited daily fluctuations of competent flows	Bank erosion and in-channel storage (lower reaches)	Low transport rates	Clockwise
Late summer/ early autumn	Glacier melt	Moderate to very high (rainfall events) Substantial daily fluctuations	Glacier and peri-glacial, and localized sources during rainfall events (tributaries)	High transport rates	Counterclockwise

on direct visual observations. This area is inactive in July as snow cover and reduced flow discharges from the glacier outlets keep it disconnected from the lower part of the basin (Figures 10c and 10d). But probably even more important is the amount of sediment transported by the sub- and supra-glacial flows (Figure 10e and 10f) which develop and enlarge

rapidly once the glacier becomes snow free and ice surface starts to melt (Davies *et al.*, 2003; Davies and Smart, 2007).

However, a certain time lag is needed for the coarse sediments from the glacier and the pro-glacial area to reach the monitoring site (located approximately 4.6 km downstream, Figure 3). Velocity of clasts of different sizes is being investigated in the Saldur River using passive integrated transponders (PIT) inserted in natural particles and by stationary antennas placed in a reach upstream of the LSG. From these experiments we expect to gain more insight into the daily time lag between water and sediment fluxes. For the moment, we argue that the complex alternation between clockwise and counterclockwise hysteresis patterns during the late glacier melt period is likely the result of the superimposition of water discharge fluctuations – daily flow peaks translates downstream at a celerity of about 2 m s^{-1} from the upper stream gauge (USG) to the LSG – on slower sediment waves originated each day at the upper part of the channel. Previous studies (Lisle *et al.*, 2001; Sklar *et al.*, 2009) showed that sediment input to a river system moves downstream as a pulse, with a combined effect of translation and dispersion depending on sediment input rate and size. Lane *et al.* (1996) showed that at a certain distance from the pro-glacial area of the Haut Glacier d'Arolla in the Pennine Alps (Switzerland), sediment was supplied with a temporal lag which resulted in higher sediment transport during the falling limb of glacier melt hydrographs (i.e. counterclockwise hysteresis). However, as Lane *et al.* (1996) pointed out, a complex set of channel changes and downstream travel of sediment waves dynamics are responsible for the relative daily timing of discharge and sediment flux. Indeed, sediment supply and transfer processes variability at a variety of spatial and timescales determine the bedload transport generated by a single flood event (e.g. Reid *et al.*, 2007; Raven *et al.*, 2009), making particularly complex to differentiate the source of sediment (Johnson and Warburton, 2006). However, even though the Saldur River was not monitored in terms of sub-daily cross-section dynamics as in Lane *et al.* (1996), repeated topographic surveys and visual observations carried out from 2011 to 2013 indicate a high channel stability, with very limited change with each summer and from year-to-year, also in the braided section located approximately 3 km upstream of the LSG (see Figures 2 and 3). Therefore it seems that glacial and peri-glacial sediments are the main responsibility for the different late summer hysteresis cycles, as well as for its augmented bedload transport as discussed in the next section. Figure 11 intends to summarize our observations on the different water and sediment origins occurring during snowmelt and late glacier melt in the Saldur basin, which are reckoned responsible for the different hysteretic patterns described earlier. Generally, in the Saldur the sediment particles originating at the pro-glacial area during late August and September moving at the lower velocity range are likely to be stored within the lower channel through the winter as competent flows usually end in mid-October. These are thereafter readily available for transport in late May–early June, as soon as snowmelt starts again. Dominance of clockwise hysteresis pattern during snowmelt period reveals both the delivery of sediments from areas close to the measurement point and the remobilization of sediment previously deposited in the channel (e.g. Williams, 1989; Seeger *et al.*, 2004; Langlois *et al.*, 2005). Unfortunately, the geophone was not operational during June 2011 and thus the hysteresis during the early snowmelt remains unknown.

Bedload availability, transport rates and perspectives

Location and seasonal dynamics – governed by snow cover – of sediment availability in the Saldur basin appears to be rather complex due to the superimposition of different runoff generation and sediment sources, which give rise to varying hysteretic loops moving from July to September. The analysis of the number of bedload impulses per unit of time (i.e. uncalibrated bedload intensity) in relation to water discharge

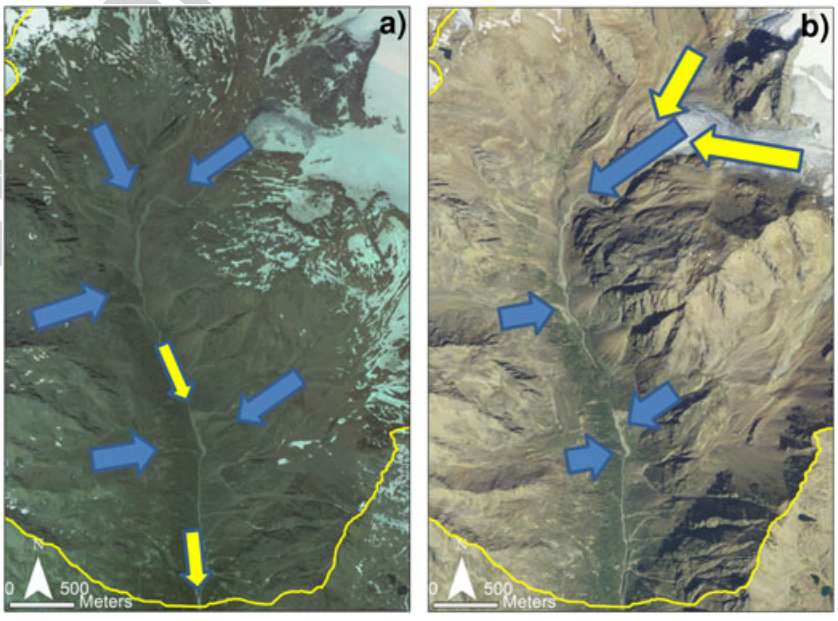

Colour online, B&W in print

Figure 11. Sketch summarizing our observations on the main seasonal changes in dominant runoff and sediment sources in the Saldur River basin. Blue and yellow arrows illustrate the location of the main water and sediment sources, respectively responsible for daily fluctuations and thus hysteresis cycles: (a) during the snowmelt-dominated period (June to July) runoff is generated in a large part of the basin, whereas available coarse sediment comes from either unstructured patches in the lower channel bed and from bank erosions in the lower reaches; (b) during periods dominated by glacier melt (late August and September), daily runoff fluctuations as well as most sediment input originates mostly from the glacier and the peri-glacial area, apart from the case of intense rainfall events where tributaries (see Figure 10b) may become relevant.

can help understand whether bedload rates are also different based on the dominant runoff origin. Indeed, such analysis (carried out using channel 4 of the pipe sensor) shows (Figure 9) that bedload impulses recorded during late glacier melt (September) plot generally well higher than those in August and July (snowmelt dominated period).

This evidence – consistent with results coming from direct bedload samples collected from 2011 to 2013 (Comiti *et al.*, 2013) – seems to indicate that clockwise loops (commonly associated to readily available sediments) are not necessarily associated to higher bedload transport intensities, which depend on actual sediment volumes made available per unit of time. Clearly, the time lag for entrained sediments (i.e. from banks, bed and from glacial and peri-glacial areas) with respect to water flux at any potential measuring station depends on the location of the station and on the differences in average velocity between water and sediment particles (e.g. Tena et al.,). Therefore, hysteresis patterns would be very likely different if measured in other reaches of the Saldur River. For instance, at the glacier mouth hysteresis loops could be even absent in the late glacier melt period, implying unlimited sediment supply and comparable sediment transport rates in both rising and falling limbs of daily hydrographs. However, the relationship between water and bedload rates during glacier melt in the lower reaches of the Saldur River, tens of kilometres downstream of the LSG, is expected to be quite different from that observed at our measuring station, but hardly predictable without a good understanding of bedload particles kinematics from the glacial/peri-glacial origin down to in-channel transfer.

A potential limitation on the interpretation of bedload hysteresis in our study site is the fact that the number of impulses collected by the pipe sensor depend – as with other indirect methods – not only on the number of particles hitting the pipe within a given interval, but also on the mode of particle movement (sliding versus rolling) and on the size of the particles as well. Particle size can actually affect the signal registered by the pipe sensor in a way that may alter hysteretic trends. For instance, the brakeage of a static armour layer during the rising limb of a flood event (e.g. Vericat *et al.*, 2006), or change in roughness (Gaeuman, 2010) or mobility of finer sediments during an event (Mao, 2012) could actually change the size of transported particles at the same discharge before and after the hydrograph peak.

Although direct bedload measurements are needed to quantify actual transport rates, because of the very strong non-linearity, temporal variability and hysteresis of bedload, occasional samples could provide misleading information about the complex process of bedload discharge. This suggests that bedload samples should be taken during seasons characterized by different runoff generation processes, and during rising and falling limb of hydrographs.

Indirect bedload measurements confirm the remarkable potential of allowing exploration of sediment processes at a scale larger than single cross-sections, providing the opportunity to infer dynamic of sediment sources at the basin scale from relatively inexpensive at-a-station measurements. Especially if taken continuously for a long period of time, indirect bedload measurements could provide invaluable insights into the dynamics of glacier melt and related sediment production. Alpine glaciers are particularly sensitive to climate change (Zemp *et al.*, 2007; Huss *et al.*, 2010), with fast retreat and an earlier disappearance of residual snow cover in the season. Therefore, longer and warmer glacier melt periods could likely result in higher sediment delivery to the Saldur River, in a manner that could be revealed by a change in the dominant daily hysteretic pattern. Long-term studies are definitely needed to unravel catchment response to hydroclimatic changes, especially if mediated by a glacier. The results from this study suggest that bedload dynamics can be substantially different in periods with snowmelt and glacier melt as a result of complex superimposition of sediment sources and sediment delivery acting at different time and spatial scales. One year of observations is long enough only to realize the complexity of bedload transport in a small glacier-fed basin, but these results point to the chance of using hysteretic patterns to infer sediment transport dynamics and to use these interpretations to guide sound indirect bedload calibration strategies.

Limits in the interpretation of bedload hysteretical patterns

Most of the existing literature on hysteresis cycles in sediment transport has associated clockwise loops to the presence of ready available sediments, whereas counterclockwise cycles are explained by events which increase sediment supply after the flood peak has occurred (e.g. the breakage of armour layers). Even if reasonable, evidence supporting this dominant interpretation tends to be generally qualitative and lacking field verification especially when bedload transport is considered. Remarkably, the spatio-temporal dimensions lying behind field-derived data (typically at one cross-section only) on water-sediment curves (and thus on sediment hysteresis loops) have been generally overlooked. In particular, the effects of the inherent 'kinematic delay' due to the time lag between water and sediment waves – most likely larger for bedload than for suspended transport, as its velocity relative to water flow are lower for the former – have not been sufficiently taken into account, and thus the consequent longitudinal variations in the hysteretic cycles during the same flow event have not been investigated, also because their documentation would require multiple bedload observation sites at different locations along a channel (Tena et al.,). However, the same variations in shape and orientation of hysteretic loops are expected at the seasonal scale if the location of active sediment sources changes through time, as it is the case of glacier-fed rivers where high-elevation, distant source become active only during the late summer, and are controlled by progressive snowpack disappearance. Therefore, the complexity of factors governing the temporal relationship between water and sediment transport rates in such river systems make conventional interpretations inapplicable, and indeed simplified conclusions cannot be made with confidence.

Likewise, our interpretation of hysteresis cycles in the Saldur River should be verified through more detailed field surveys. For instance, we interpret clockwise hysteresis during snowmelt to the supply of sediment by bank erosion processes occurring next to the measuring station. However, the exact localization, magnitude, and timing of bank collapses should be known to truly verify this hypothesis, along with the assessment of virtual travel times of sediments. Also, sediment arrangement and cluster development before and after each daily discharge fluctuation should be assessed, e.g. using a (bathymetric) terrestrial laser scanner, which has the potential to permit the assessment of differences in roughness, imbrication and orientation at the grain and cluster scales (Hodge *et al.*, 2009; Mao, 2012).

Still, the fact that some daily discharge fluctuations exhibit counterclockwise hysteresis during snowmelt has not a straightforward explanation, and could be due to complete exhaustion of loose sediments during the falling limb of a

previous event. However, the sparse clockwise events during the late glacier melt period could be due to temporal storage of sediments in proximity of the monitoring station, possibly due to an antecedent event featuring characteristics (e.g. duration and magnitude) which led to relatively more deposition there. Overall, sediment availability from upstream reaches, and composition and stability of the bed surface layer is strongly time-dependent in active river systems such as glacier-fed rivers. As the sediment flux response to a flow event is due to a complex set of dominant constraints, a proper determination of causes of hysteresis would imply a detailed, frequent monitoring of magnitude and timing of sediment sources, sediment storage and transfer along the stream, as well as of the degree of sediment organization on the bed. These requirements challenge our current ability to monitor these variables at the timescales needed to explore these processes, but definitely point out to a set of research goals needed for a better understanding of these river systems, which are subject to rapid environmental changes.

Conclusions

Bedload transport is a complex process which depends on the flow competence and availability of sediments. Because the degree of sediment availability can change before and after the occurrence of peak discharge during flood events, bedload hysteretic patterns can appear, revealing peak discharge anticipating the peak of bedload transport rate (clockwise hysteresis) or the opposite (counterclockwise hysteresis). Evidence provided by an acoustic pipe sensor installed in the Saldur River suggests that bedload dynamics vary seasonally due to different dominant runoff generation processes. Clockwise hysteretic patterns are relatively more abundant during snowmelt periods possibly due to both the activation of sediments sources (bank erosion) in the lower part of the basin near to the monitoring station and unpacked bed surface sediments. Counterclockwise hysteresis are instead relatively more frequent during late glacier melt periods, and likely related to the supply of sediments from the glacier and from the peri-glacial areas, which are much farther from the monitoring station than sources active earlier in the summer. Indeed, because data from the acoustic sensor show that bedload rates are higher during glacier melt than in the snow melt period, sediment availability seems not necessarily related to actual bedload transport but to the degree of activity and location of sediment sources. This study emphasizes the usefulness of indirect bedload measurements for assessing the temporal variability of bedload transport in mountain rivers, as well as for inferring the activation of sediment sources at the basin scale. At the same time, this research shows that bedload dynamics in glacierized basins is affected by the complex interactions among runoff, sediment availability and bed organization, all of which are strongly time-dependent at different temporal and spatial scales. Therefore, we believe that our current ability to make reliable predictions on future morphological changes in similar river systems is very limited, and further field investigations coupling bedload and runoff generation monitoring to detailed morphological analysis are highly needed.

Acknowledgements—This work was financially supported by the research projects 'Effects of climate change on high-altitude ecosystems: monitoring the Upper Match Valley' (Free University of Bozen-Bolzano), 'EMERGE: Retreating glaciers and emerging ecosystems in the Southern Alps' (Herzog-Sellenberg- und Ritter-Stiftung im Stifterverband für die Deutsche Wissenschaft) and 'GESTO: Gestione del trasporto di sedimento nei piccoli bacini montani' (Autonomous Province of Bozen-Bolzano). Technical support was given by the Department of Hydraulic Engineering and Hydrographic Office of the Autonomous Province of Bozen-Bolzano. Comments by John Laronne, by an anonymous reviewer and by Stuart Lane greatly helped to improve the original manuscript.

References

Alexandrov Y, Laronne JB, Reid I. 2007. Intra-event and inter-seasonal behaviour of suspended sediment in flash floods of the semi-arid northern Negev, Israel. *Geomorphology* **85**(1–2): 85–97.

Araujo HA, Cooper AB, Hassan MA, Venditti J. 2012. Estimating suspended sediment concentrations in areas with limited hydrological data using a mixed-effects model. *Hydrological Processes* **26**: 3678–3688. DOI. 10.1002/hyp.8462

Best H, McNamara JP, Liberty L. 2005. Association of ice and river channel morphology determined using groundpenetrating radar in the Kuparuk River, Alaska. *Arctic, Antarctic, and Alpine Research* **37**(2):157–162.

Beylich AA, Sandberg O, Molau U, Wache S. 2006. Intensity and spatio-temporal variability of fluvial sediment transfers in an Arctic-oceanic periglacial environment in northernmost Swedish Lapland (Latnjavagge catchment). *Geomorphology* **80**: 114–130.

Boeckli L, Brenning A, Gruber S, Noetzli J. 2011. A statistical permafrost distribution model for the European Alps. *The Cryosphere Discussions* **5**: 1419–1459.

Bunte K, Abt SR, Potyondy JP, Ryan SE. 2004. Measurement of coarse gravel and cobble transport using portable bedload traps. *Journal of Hydraulic Engineering* **130**(9): 879–893.

Comiti F, Cadol D, Wohl EE. 2009. Flow regimes, bed morphology, and flow resistance in self-formed step-pool channels. *Water Resources Research* **45**: W04424. DOI. 10.1029/2008WR007259.

Comiti F, Dell'Agnese F, Mao L, Engel M, Lucia A, Penna D, Bertoldi G. 2013. Temporal variations of bedload transport in a glacierized mountain basin. *Proceedings,8th IAG International Conference on Geomorphology, 27–31 August*, Paris.

D'Agostino V, Lenzi MA. 1999. Bedload transport in the instrumented catchment of the Rio Cordon: part II. Analysis of the bedload rate. *Catena* **36**: 191–204.

Davies TR, Smart CC. 2007. Obstruction of subglacial conduits by bedload sediment – implications for alpine glacier motion. *Journal of Hydrology (NZ)* **46**(2): 51–62.

Davies TRH, Smart CC, Turnbull JM. 2003. Water and sediment outbursts from advanced Franz Josef glacier, New Zealand. *Earth Surface Processes and Landforms* **28**: 1081–1096.

Engel M, Comiti F, Penna D, Notarnicola C, Niedrist G, Bertoldi G. 2013. Snow modelling in a glacierized catchment using scale-dependent calibration data. *Proceedings, EGU General Assembly, 7–12 April 2013*, Vienna; Vol. 15, EGU2013-674.

Fuller C, Willett SD, Slingerland R, Hovius N. 2003. A stochastic model of sediment supply, transport and storage in a Taiwan mountain drainage basin. *Journal of Geology* **111**(1): 71–88.

Gaeuman D. 2010. Mechanics of bedload rating curve shifts and bedload hysteresis in the Trinity River, California. *Paper presented at 2nd Joint Federal Interagency Conference on Sedimentation and Hydrologic Modeling, Advisory Committee on Water Information*, Las Vegas, NV.

Giménez R, Casalí J, Grande I, Díez J, Campo MA, Álvarez-Mozos J, Goni M. 2012. Factors controlling sediment export in a small agricultural watershed in Navarre (Spain). *Agricultural Water Management* **110**: 1–8.

Gray JR, Laronne JB, Marr JDG. 2010. *Bedload-surrogate Monitoring Technologies*, US Geological Survey Scientific Investigations Report 2010–5091. US Geological Survey: Reston, VA; 37 pp. http://pubs.usgs.gov/sir/2010/5091

Habersack HM, Nachtnebel HP, Laronne JB. 2001. The continuous measurement of bedload discharge in a large alpine gravel bed river. *Journal of Hydraulic Research* **39**: 125–133. DOI. 10.1080/00221680109499813

Hassan MA, Roey E, Parker G. 2006. Experiments on the effect of hydrograph characteristics on vertical grain sorting in gravel bed

rivers. *Water Resources Research* **42**: W09408. DOI. 10.1029/2005WR004707

Hodge R, Brasington J, Richards K. 2009. Analysing laser-scanned digital terrain models of gravel bed surfaces: linking morphology to sediment transport processes and hydraulics. *Sedimentology* **56**(7): 2024–2043.

Horowitz A. 2003. An evaluation of sediment rating curves for estimating SSC for subsequent flux calculations. *Hydrological Processes* **17**: 3387–3409.

Hudson PF. 2003. Event sequence and sediment exhaustion in the lower Panuco Basin, Mexico. *Catena* **52**: 57–76.

Humphries R, Venditti JG, Sklar LS, Wooster JK. 2012. Experimental evidence for the effect of hydrographs on sediment pulse dynamics in gravel-bedded rivers. *Water Resources Research* **48**: W01533. DOI. 10.1029/2011WR010419

Huss M, Hock R, Bauder A, Funk M. 2010. 100-year glacier mass changes in the Swiss Alps linked to the Atlantic Multidecadal Oscillation. *Geophysical Research Letters* **37**: L10501. DOI. 10.1029/2010GL042616

Iida T, Kajihara A, Okubo H, Okajima K. 2012. Effect of seasonal snow cover on suspended sediment runoff in a mountainous catchment. *Journal of Hydrology* **428–429**: 116–128.

Johnson RM, Warburton J. 2006. Variability in sediment supply, transfer and deposition in an upland torrent system: Iron Crag, northern England. *Earth Surface Processes and Landforms* **31**: 844–861.

Klein M. 1984. Anti-clockwise hysteresis in suspended sediment concentration during individual storms: Holbeck catchment; Yorkshire, England. *Catena* **11**: 251–257.

Kuhnle RA. 1992. Bed load transport during rising and falling stages on two small streams. *Earth Surface Processes and Landforms* **17**: 191–197. DOI. 10.1002/esp.3290170206

Kwaad FJPM. 1991. Summer and winter regimes of runoff generation and soil erosion on cultivated loess soils (The Netherlands). *Earth Surface Processes and Landforms* **16**: 653–662.

Lana-Renault N, Alvera B, García-Ruiz JM. 2011. Runoff and sediment transport during the snowmelt period in a Mediterranean high mountain catchment. *Arctic, Antarctic, and Alpine Research* **42**(2): 213–222.

Lane S, Richards K, Chandler J. 1996. Discharge and sediment supply controls on erosion and deposition in a dynamic alluvial channel. *Geomorphology* **15**(1): 1–15.

Langlois JL, Johnson DW, Mehuys GR. 2005. Suspended sediment dynamics associated with snowmelt runoff in a small mountain stream of Lake Tahoe (Nevada). *Hydrological Processes* **19**: 3569–3580.

Lee KT, Liu Y-L, Cheng K-H. 2004. Experimental investigation of bedload transport processes under unsteady flow conditions. *Hydrological Processes* **18**: 2439–2454. DOI. 10.1002/hyp.1473

Lenzi MA. 2001. Step-pool evolution in the Rio Cordon, Northeastern Italy. *Earth Surface Processes and Landforms* **26**: 991–1008.

Lenzi MA, Mao L, Comiti F. 2004. Magnitude-frequency analysis of bed load data in an Alpine boulder bed stream. *Water Resources Research* **40**: W0720. DOI. 10.1029/2003WR002961

Lenzi MA, Mao L, Comiti F. 2006. When does bedload transport begin in steep boulder-bed streams? *Hydrological Processes* **20**: 3517–3533.

Lisle TE, Cui Y, Parker G, Pizzuto JE, Dodd AM. 2001. The dominance of dispersion in the evolution of bed material waves in gravel bed rivers. *Earth Surface Processes and Landforms* **26**: 1409–1420. DOI. 10.1002/esp.300

Q5 Madej MA, Sutherland DG, Lisle TE, Pryor B. 2009. Channel responses to varying sediment input: a flume experiment modeled after Redwood Creek, California. *Geomorphology* **103**(4): 507–519

Mao L. 2012. The effect of hydrographs on bed load transport and bed sediment spatial arrangement. *Journal of Geophysical Research - Earth Surface* **117**: F03024. DOI. 10.1029/2012JF002428

McDonald DM, Lamoureux SF. 2009. Hydroclimatic and channel snowpack controls over suspended sediment and grain size transport in a high arctic catchment. *Earth Surface Processes and Landforms* **34**: 424–436. DOI. 10.1002/esp.1751

McNamara JP, Borden C. 2004. Observations on the movement of coarse gravel using implanted motion-sensing radio transmitters. *Hydrological Processes* **18**: 1871–1884.

Mizuyama T, Fujita M, Nonaka M. 2003. Measurement of bed load with the use of hydrophnes in mountan rivers. In Erosion and Transport Measurement in Rivers: Technological and Methodological Advances, Bogen J, Fergus T, Walling D (eds), IAHS Publication 283. IAHS Press: Wallingford; 222–227.

Mizuyama T, Laronne JB, Nonaka M, Sawada T, Satofuka Y, Matsuoka M, Yamashita S, Sako Y, Tamaki S, Watari M, Yamaguch S, Tsuruta K. 2010a. Calibration of a passive acoustic bedload monitoring system in Japanese mountain rivers. In Bedload-surrogate Monitoring Technologies, Gray JR, Laronne JB, Marr JDG (eds), US Geological Survey Scientific Investigations Report 2010-5091. US Geological Survey: Reston, VA; 296–318.

Mizuyama T, Oda A, Laronne JB, Nonaka M, Matsuoka M. 2010b. Laboratory tests of a Japanese pipe geophone for continuous acoustic monitoring of coarse bedload. In Bedload-surrogate Monitoring Technologies, Gray JR, Laronne JB, Marr JDG (eds), US Geological Survey Scientific Investigations Report 2010-5091. US Geological Survey: Reston, VA; 319–335.

Møen KM, Bogen J, Zuta JF, Ade PK, Esbensen K. 2010. Bedload measurement in rivers using passive acoustic sensors. In Bedload-surrogate Monitoring Technologies, Gray JR, Laronne JB, Marr JDG (eds), US Geological Survey Scientific Investigations Report 2010-5091. US Geological Survey: Reston, VA; 336–351.

Montgomery DR, Buffington JM. 1997. Channel-reach morphology in mountain drainage basins. *Geological Society of America Bulletin* **109**: 591–611.

Penna D, Stenni B, Šanda M, Wrede S, Bogaard TA, Gobbi A, Borga M, Fisher BMC, Bonazza M. 2010. On the reproducibility and repeatability of laser absorption spectroscopy measurements for δ^2H and δ^{18}O isotopic analysis. *Hydrology and Earth System Sciences* **14**: 1551–1566. DOI. 10.5194/hess-14-1551-2010

Penna D, Stenni B, Šanda M, Wrede S, Bogaard TA, Michelini M, Fisher BMC, Gobbi A, Mantese N, Zuecco G, Borga M, Bonazza M, Sobotková M, Čejková B, Wassenaar LI. 2012. Technical note: evaluation of between-sample memory effects in the analysis of δ^2H and δ^{18}O water samples measured by laser spectroscopes. *Hydrology and Earth System Sciences* **16**: 3925–3933. DOI. 10.5194/hess-16-3925-2012

Penna D, Mao L, Comiti F, Engel M, Dell'Agnese A, Bertoldi G. 2013. Hydrological effects of glacier melt and snowmelt in a high-elevation catchment. *Die Bodenkultur* **64**(3–4): 93–98.

Priesnitz K, Schunke E. 2002. The fluvial morphodynamics of two small permafrost drainage basins, Richardson Mountains, northwestern Canada. *Permafrost and Periglacial Processes* **13**(3): 207–217.

Raven EK, Lane SN, Ferguson RI, Bracken LJ. 2009. The spatial and temporal patterns of aggradation in a temperate, upland, gravel-bed river. *Earth Surface Processes and Landforms* **34**(9): 181–1197.

Reid I, Frostick LE, Layman JT. 1985. The incidence and nature of bedload transport during flood flows in coarse-grained alluvial channels. *Earth Surface Processes and Landforms* **10**: 33–44. DOI. 10.1002/esp.3290100107

Reid SC, Lane SN, Berney JM, Holden J. 2007. The timing and magnitude of coarse sediment transport events within an upland, temperate gravel-bed river. *Geomorphology* **83**(1–2): 152–182.

Rickenmann D. 1994. Bedload transport and discharge in the Erlenbach Stream. In *Dynamics and Geomorphology of Mountain Rivers*, Ergenzinger P, Schmidt KH (eds), Lecture Notes in Earth System Sciences. Springer Verlag: Berlin; vol. 52, 53–66.

Rickenmann D. 2001. Comparison of bed load transport in torrents and gravel bed streams. *Water Resources Research* **37**(12): 3295–3305.

Rickenmann D, Koschni A. 2010. Sediment loads due to fluvial transport and debris flows during the 2005 flood events in Switzerland. *Hydrological Processes* **24**: 993–1007.

Rickenmann D, McArdell BW. 2007. Continuous measurement of sediment transport in the Erlenbach stream using piezoelectric bedload impact sensors. *Earth Surface Processes and Landforms* **32**: 1362–1378.

Rickenmann D, D'Agostino V, Dalla Fontana G, Lenzi M, Marchi L. 1998. New results from sediment transport measurements in two Alpine torrents. In Hydrology, Water Resources and Ecology in Headwaters, Kovar K, Tappeiner U, Peters NE, Craig RG (eds), IAHS Publication 248. IAHS Press: Wallingford; 283–289.

Rickenmann D, Turowski JM, Fritschi B, Klaiber A, Ludwig A. 2012. Bedload transport measurements at the Erlenbach stream with geophones and automated basket samplers. *Earth Surface Processes and Landforms* **37**: 1000–1011.

Seeger M, Errea MP, Begueria S, Arnaez J, Marti C, Garcia-Ruiz JM. 2004. Catchment soil moisture and rainfall characteristics as determinant factors for discharge/suspended sediment hysteretic loops in a small headwater catchment in the Spanish Pyrenees. *Journal of Hydrology* **288**: 299–311.

Sklar LS, Fadde J, Venditti JG, Nelson P, Wydzga MA, Cui Y, Dietrich WE. 2009. Translation and dispersion of sediment pulses in flume experiments simulating gravel augmentation below dams. *Water Resources Research* **45**: W08439. DOI. 10.1029/2008WR007346

Steegen A, Govers G, Nachtergaele J, Takken I, Beuselinck L, Poesen J. 2000. Sediment export by water from an agricultural catchment in the Loam Belt in central Belgium. *Geomorphology* **33**: 25–36.

Tananaev NI. 2012. Hysteresis effect in the seasonal variations in the relationship between water discharge and suspended load in rivers of permafrost zone in Siberia and Far East. *Water Resources* **39**(6): 648–656.

Q12 Tena A, Vericat D, Batalla RJ. nd. Accepted for publication. Suspended sediment dynamics during flushing flows in a large impounded river (the lower River Ebro, NE Iberian Peninsula). *Journal of Soils and Sediments*.

Turowski JM, Rickenmann D. 2009. Tools-and cover-effects in bedload transport observations in the Pitzbach, Austria. *Earth Surface Processes and Landforms* **33**: 26–37.

Turowski JM, Rickenmann D. 2010. Measuring the statistics of bed-load transport using indirect sensors. *Journal of Hydraulic Engineering* **137**(1): 116–121.

Turowski JM, Yager EM, Badoux A, Rickenmann D, Molnar P. 2009. The impact of exceptional events on erosion, bedload transport and channel stability in a step-pool channel. *Earth Surface Processes and Landforms* **34**: 1661–1673.

Vatne G, Naas ØT, Skarholen T, Beylich AA, Berthling I. 2008. Bed load transport in a steep snowmelt-dominated mountain stream as inferred from impact sensors. *Norsk Geografisk Tidsskrift-Norwegian Journal of Geography* **62**(2): 66–74.

Vericat D, Batalla RJ, Garcia C. 2006. Breakup and re-establishment of the armor layer in a highly regulated large gravel-bed river: the lower Ebro. *Geomorphology* **76**: 122–136.

Wilcock PR, Kenworthy ST, Crowe JC. 2001. Experimental study of the transport of mixed sand and gravel. *Water Resources Research* **37**: 3349–3358.

Williams GP. 1989. Sediment concentration versus water discharge during single hydrologic events in rivers. *Journal of Hydrology* **111**(1–4): 89–106.

Wulf H, Bookhagen B, Scherler D. 2012. Climatic and geologic controls on suspended sediment flux in the Sutlej River Valley, western Himalaya. *Hydrology and Earth System Sciences* **16**: 2193–2217.

Zemp M, Hoelzle M, Haeberli W. 2007. Distributed modelling of the regional climatic equilibrium line altitude of glaciers in the European Alps. *Global and Planetary Change* **56**: 83–100.

Zimmermann A, Church M, Hassan MA. 2010. Step-pool stability: testing the jammed state hypothesis. *Journal of Geophysical Research - Earth Surface* **115**: F02008. DOI. 10.1029/2009JF001365.

Author Query Form

Journal: Earth Surface Processes and Landforms

Article: esp_3563

Dear Author,

During the copyediting of your paper, the following queries arose. Please respond to these by annotating your proofs with the necessary changes/additions.

- If you intend to annotate your proof electronically, please refer to the E-annotation guidelines.
- If you intend to annotate your proof by means of hard-copy mark-up, please refer to the proof mark-up symbols guidelines. If manually writing corrections on your proof and returning it by fax, do not write too close to the edge of the paper. Please remember that illegible mark-ups may delay publication.

Whether you opt for hard-copy or electronic annotation of your proofs, we recommend that you provide additional clarification of answers to queries by entering your answers on the query sheet, in addition to the text mark-up.

Query No.	Query	Remark
Q1	AUTHOR: "Forbes and Lamoureux (2005)" is cited in text but not given in the reference list. Please provide details in the list or delete the citation from the text.	
Q2	AUTHOR: The citation "Tena et al., accepted for publication" (original) has been changed to "Tena et al., nd". Please check if appropriate.	
Q3	AUTHOR: The citation "Tena et al., accepted for publication" (original) has been changed to "Tena et al., nd". Please check if appropriate.	
Q4	AUTHOR: Reference "Beylich et al. (2006)" is not cited in the text. Please indicate where it should be cited; or delete from the reference list.	
Q5	AUTHOR: Reference "Madej et al. (2009)" is not cited in the text. Please indicate where it should be cited; or delete from the reference list.	
Q6	AUTHOR: Lenzi et al., 2001 has been changed to Lenzi, 2001 to match the reference list, please confirm or correct.	
Q7	AUTHOR: Please confirm '10 °C' rather than '10°', or clarify	
Q8	AUTHOR: Turowski and Rickenmann, 2011 has been changed to Turowski and Rickenmann, 2010 to match the reference list, please confirm or correct.	
Q9	AUTHOR: Please provide full reference details for Habler et al., 2009.	
Q10	AUTHOR: Please confirm definition of USG, or correct.	
Q11	AUTHOR: Please provide any update for Tena et al., if posible.	
Q12	AUTHOR: Please provide any update for Tena et al., i.e. DOI number, volume number, page range, etc.	

WILEY-BLACKWELL

USING e-ANNOTATION TOOLS FOR ELECTRONIC PROOF CORRECTION

Required software to e-Annotate PDFs: Adobe Acrobat Professional or Adobe Reader (version 7.0 or above). (Note that this document uses screenshots from Adobe Reader X)
The latest version of Acrobat Reader can be downloaded for free at: http://get.adobe.com/uk/reader/

Once you have Acrobat Reader open on your computer, click on the Comment tab at the right of the toolbar:

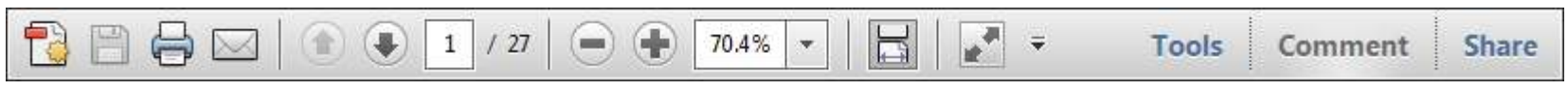

This will open up a panel down the right side of the document. The majority of tools you will use for annotating your proof will be in the Annotations section, pictured opposite. We've picked out some of these tools below:

1. Replace (Ins) Tool – for replacing text.

Strikes a line through text and opens up a text box where replacement text can be entered.

How to use it

- Highlight a word or sentence.
- Click on the Replace (Ins) icon in the Annotations section.
- Type the replacement text into the blue box that appears.

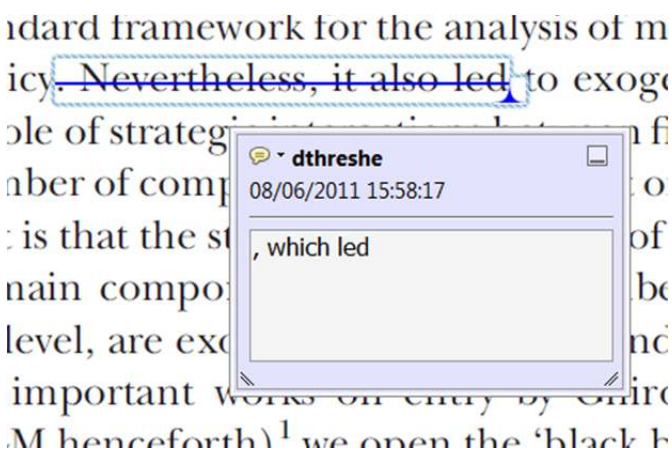

2. Strikethrough (Del) Tool – for deleting text.

Strikes a red line through text that is to be deleted.

How to use it

- Highlight a word or sentence.
- Click on the Strikethrough (Del) icon in the Annotations section.

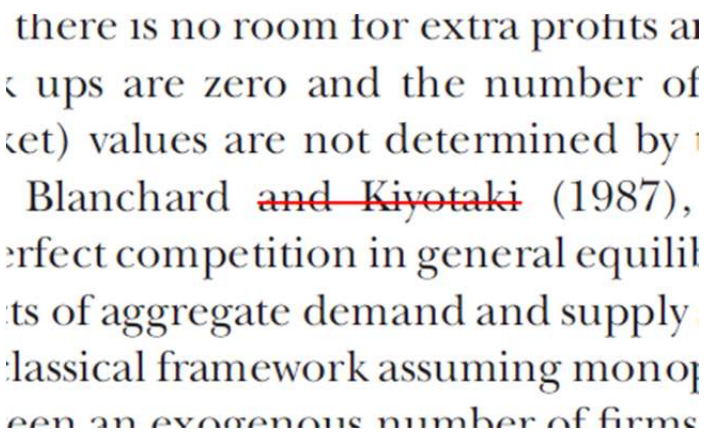

3. Add note to text Tool – for highlighting a section to be changed to bold or italic.

Highlights text in yellow and opens up a text box where comments can be entered.

How to use it

- Highlight the relevant section of text.
- Click on the Add note to text icon in the Annotations section.
- Type instruction on what should be changed regarding the text into the yellow box that appears.

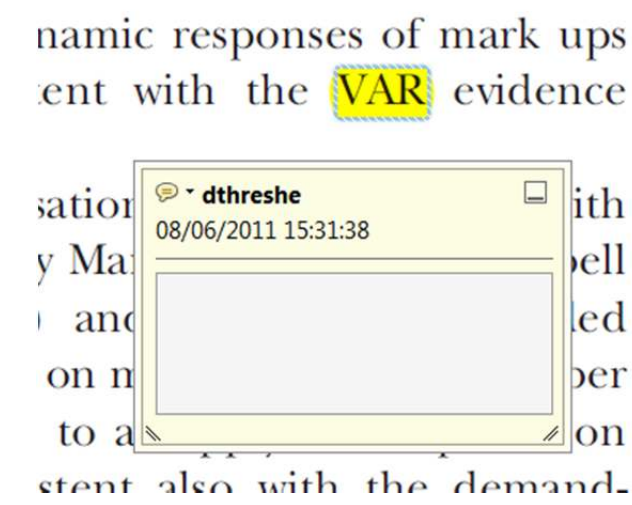

4. Add sticky note Tool – for making notes at specific points in the text.

Marks a point in the proof where a comment needs to be highlighted.

How to use it

- Click on the Add sticky note icon in the Annotations section.
- Click at the point in the proof where the comment should be inserted.
- Type the comment into the yellow box that appears.

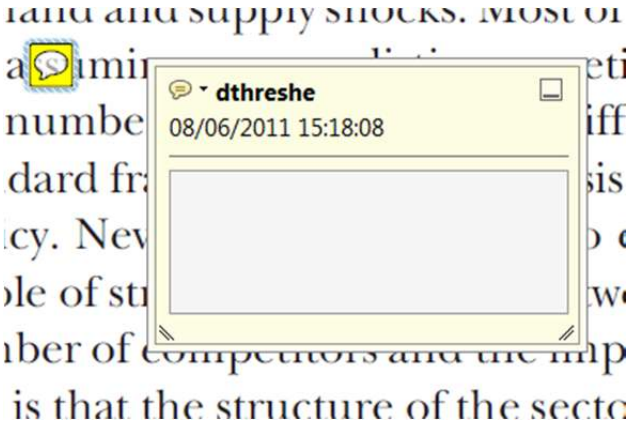

WILEY-BLACKWELL

USING e-ANNOTATION TOOLS FOR ELECTRONIC PROOF CORRECTION

5. Attach File Tool – for inserting large amounts of text or replacement figures.

Inserts an icon linking to the attached file in the appropriate pace in the text.

How to use it

- Click on the Attach File icon in the Annotations section.
- Click on the proof to where you'd like the attached file to be linked.
- Select the file to be attached from your computer or network.
- Select the colour and type of icon that will appear in the proof. Click OK.

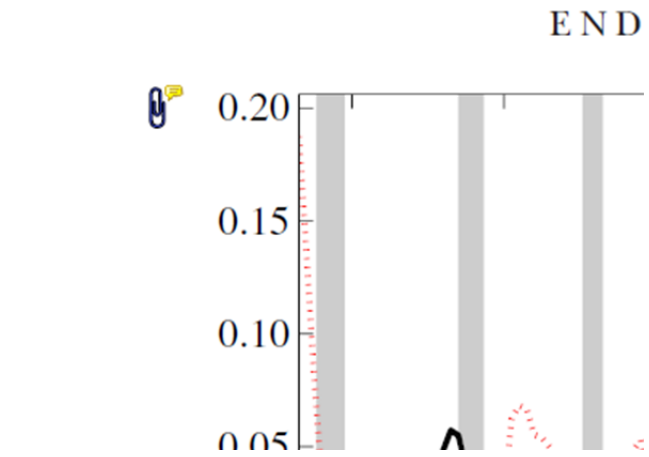

6. Add stamp Tool – for approving a proof if no corrections are required.

Inserts a selected stamp onto an appropriate place in the proof.

How to use it

- Click on the Add stamp icon in the Annotations section.
- Select the stamp you want to use. (The Approved stamp is usually available directly in the menu that appears).
- Click on the proof where you'd like the stamp to appear. (Where a proof is to be approved as it is, this would normally be on the first page).

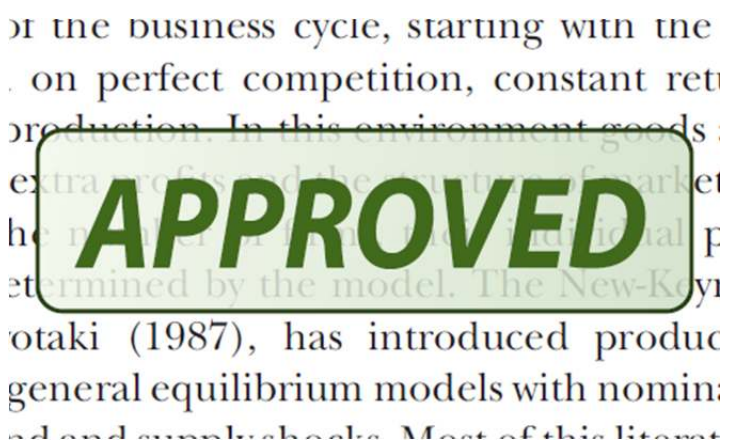

7. Drawing Markups Tools – for drawing shapes, lines and freeform annotations on proofs and commenting on these marks.

Allows shapes, lines and freeform annotations to be drawn on proofs and for comment to be made on these marks..

How to use it

- Click on one of the shapes in the Drawing Markups section.
- Click on the proof at the relevant point and draw the selected shape with the cursor.
- To add a comment to the drawn shape, move the cursor over the shape until an arrowhead appears.
- Double click on the shape and type any text in the red box that appears.

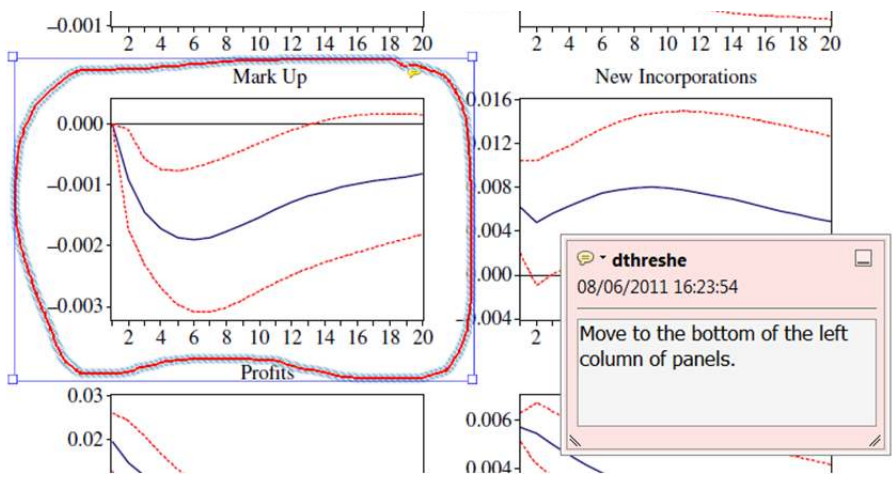

For further information on how to annotate proofs, click on the Help menu to reveal a list of further options: